Available online at www.sciencedirect.com

ScienceDirect

Energy Procedia 94 (2016) 249 – 260

Energy Procedia

13th Deep Sea Offshore Wind R&D Conference, EERA DeepWind'2016, 20-22 January 2016, Trondheim, Norway

Probabilistic assessment of floating wind turbine access by catamaran vessel

Michele Martini, Alfonso Jurado, Raúl Guanche*, Iñigo Losada

Environmental Hydraulics Institute "IH Cantabria", C/Isabel Torres 15, Santander 39011, Spain

Abstract

In this work, it is evaluated the accessibility of a floating platform, by means of a catamaran vessel equipped with a fender. The two bodies are modelled as a constrained multi-body system in the frequency domain. Transfer functions are calculated for the motions and forces of the system. Access is possible when no slip conditions occur at the fender, and when the relative rotations between the two bodies are within certain tolerance limits. Four response variables are defined to impose such conditions. In a short-term sea state the extreme maximum crest height of these variables is computed, assuming that response crest heights follow a Rayleigh distribution. Each of the extreme values is compared to a specific threshold, to determine whether access is possible or not. Accessibility is calculated for a sample platform located off the coast of Scotland using hindcast data for the period 1980-2013. Average accessibility resulted to be 23.7%. A strong seasonality is ascertained, together with a large variation of accessibility, due to the variability of wave climate.

Peer-review under responsibility of SINTEF Energi AS

Keywords: floating wind turbines; offshore accessibility; catamaran landing; walk-to-work;

* Corresponding author. Tel.:+34-942-201616; fax:+34-942-266361.

Peer-review under responsibility of SINTEF Energi AS
doi:10.1016/j.egypro.2016.09.233

1. Introduction

1.1. Offshore wind market evolution

At the end of June 2015, the offshore wind capacity installed in European waters surpassed 10 GW [1], confirming the growing trend of the previous years. The majority of the farms is located in the North Sea, where high wind speeds and a large shallow water continental shelf boosted the installation of turbines over fixed foundations. Nevertheless, in recent years the interest of offshore and energy industries towards floating wind turbines has significantly grown. These systems allow to harness energy far offshore, where wind tends to be more sustained and less turbulent, also in deep waters which are not economically exploitable by conventional fixed turbines [2]. Few full-scale prototypes have been installed and performed well during different operating conditions, encouraging the respective developers to planning the first floating wind farms [3][4][5]. These technologies may unfold a vast potential market: 66% of the North Sea itself has a water depth between 50 m and 220 m and many other regions with high power demand present similar characteristics (Mediterranean Sea, Atlantic Sea, US Pacific coast, Japan).

1.2. The availability challenge

The availability of a wind turbine is defined as the percentage of time it is able to generate electricity. In order to reach high values of availability, downtimes need to be shortened and, when possible, prevented. This is achieved through inspection and maintenance (either preventive or corrective), activities are known to affect significantly the final cost of energy (up to 25%, [6]). Costs and risks are expected to be higher for floating wind turbines, due to the short experience with real-scale systems and the added complexity brought by the platform motion [7]. For inspection and light repair, access to offshore wind turbines is usually guaranteed by means of catamarans equipped with fender or larger vessels mounting a motion-compensated gangway. In both cases, technicians walk directly from the vessel to a ladder mounted on the wind turbine structure. A number of guidelines exist to ensure that these activities would take place within certain safety limits [8]–[10]. Appropriate modelling tools are also necessary, in order to optimize maintenance strategies and identify limiting sea states for which access is possible.

1.3. Motivation

The aim of this work is to evaluate numerically the accessibility of a floating wind turbine by means of a catamaran vessel, in a walk-to-work configuration. Motivation for this effort comes mainly from the following points:

- The offshore wind energy trends and the potential market for floating turbines.
- The high costs and risks associated with operation and maintenance of offshore wind farms.
- The lack of modelling tools for walk-to-work access of floating platforms.

Previous studies, both numerical and experimental [11], [12], dealt only with fixed wind turbines and cannot be applied to the analysis of floating systems.

2. Methodology

Catamaran Crew Transfer Vessels (CTVs) are used to transfer small groups of technicians for inspection and light maintenance purposes. As it approaches the wind turbine, the catamaran docks on a boat landing structure and pushes on it through a bow-mounted fender, which absorbs the energy of the impact and provides friction to impede vertical motion. Workers access the wind turbine stepping over from the vessel and holding on a ladder. Access is possible when no-slip conditions occur at the fender, which acts as a joint from the kinematic point of view.

2.1. Analysis of a constrained multi-body hydrodynamic system

The system composed by the CTV and the floating wind turbine is modelled as a constrained, multi-body system in the frequency domain. Each body has six degrees of freedom, assembled in a frequency-dependent displacement vector $\boldsymbol{\zeta}$ (the first six elements refer to the vessel, the last six to the platform). Motions are expressed in body coordinate systems; Figure 1, shows the position of the vessel with respect to the platform, and the respective coordinate systems (apex "v" refers to the vessel, "p" to the platform"). The contact point is indicated with the symbol *C*.

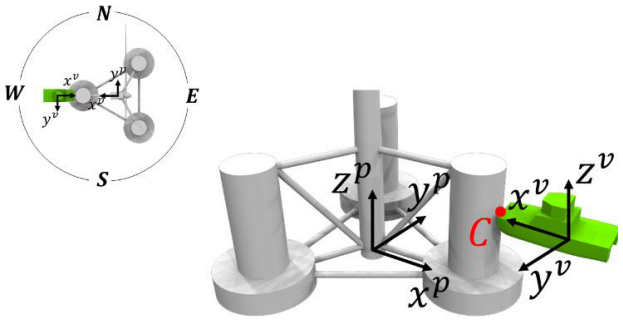

Figure 1: Coordinate systems used for multi-body modelling.

For a free-floating system, the equation of motion is written as [13], [14]:

$$\boldsymbol{G}(j\omega)\boldsymbol{\zeta}(j\omega) = \boldsymbol{f}(j\omega,\theta) \tag{1}$$

being:

$$\boldsymbol{G}(j\omega) = -\omega^2[\boldsymbol{M} + \boldsymbol{A}(\omega)] + j\omega[\boldsymbol{B}(\omega) + \boldsymbol{B}_l] + [\boldsymbol{C} + \boldsymbol{C}_l] \tag{2}$$

Above, j is the imaginary unit, ω the wave angular frequency and θ the wave direction; $\boldsymbol{M}$ is matrix of mass and inertia coefficients, $\boldsymbol{A}$ the matrix of added mass coefficients, $\boldsymbol{B}$ the matrix of potential damping coefficients, $\boldsymbol{B}_l$ the matrix of linearized damping coefficients, $\boldsymbol{C}$ the matrix of hydrostatic stiffness coefficients, $\boldsymbol{C}_l$ the matrix of linearized stiffness coefficients and $\boldsymbol{f}$ the vector of complex excitation wave force coefficients. In this work, the potential flow solver HydroD (DNV Sesam) is used to calculate the matrices $\boldsymbol{A}$, $\boldsymbol{B}$, $\boldsymbol{C}$ and the vector $\boldsymbol{f}$.

The matrices $\boldsymbol{B}_l$ and $\boldsymbol{C}_l$ are introduced due to the linear force-displacement relationship imposed by frequency domain modelling. In this work, two non-linear phenomena are considered: viscous drag (for either the vessel or the platform) and catenary mooring action (for the platform). Quadratic damping coefficients are often calculated, through either physical or numerical modelling, to model drag forces. Equivalent linear damping coefficients can then be calculated, for small displacements, using the harmonic linearization method [15], [16] giving the linearized damping matrix $\boldsymbol{B}_l$. The mooring forces are linearized using a finite difference scheme with quasi-static catenary equations [17], about an equilibrium point in which the vessel bollard push and the mooring system reaction balance out. Equivalent linear stiffness coefficients are then computed to obtain the linearized stiffness matrix $\boldsymbol{C}_l$.

When the system undergoes some kinematic constraints, the equation of motion is rewritten as [18]:

$$\begin{bmatrix} \boldsymbol{G} & \boldsymbol{D}^T \\ \boldsymbol{D} & \boldsymbol{0} \end{bmatrix} \begin{Bmatrix} \boldsymbol{\zeta} \\ \boldsymbol{\lambda} \end{Bmatrix} = \begin{Bmatrix} \boldsymbol{f} \\ \boldsymbol{0} \end{Bmatrix} \tag{3}$$

where $\boldsymbol{D}$ is the constraint matrix and $\boldsymbol{\lambda}$ the vector of resulting joint forces. The fender is modelled as a ball joint, i.e. it does not allow relative translations between the two bodies. Considering the coordinate systems defined in Figure 1, the constraint matrix is written as:

$$\boldsymbol{D} = \begin{bmatrix} 1 & 0 & 0 & 0 & +z_C^v & -y_C^v & 1 & 0 & 0 & 0 & +z_C^p & -y_C^p \\ 0 & 1 & 0 & -z_C^v & 0 & +x_C^v & 0 & 1 & 0 & -z_C^p & 0 & +x_C^p \\ 0 & 0 & 1 & +y_C^v & -x_C^v & 0 & 0 & 0 & -1 & -y_C^p & +x_C^p & 0 \end{bmatrix} \tag{4}$$

where x_C, y_C and z_C are the coordinates of the contact point. Solving Equation (3) gives the transfer functions between the wave elevation process and the displacements/reaction forces of the system.

2.2. Calculation of short-term extreme maxima

Under the hypothesis of linear force-displacement relationship the variance of a response variable x, σ_x, for a short-term stationary sea state can be calculated as:

$$\sigma_x = \int_0^{2\pi} \int_0^{\infty} \left| H_{\eta x}(j\omega,\theta) \right|^2 S_{\eta\eta}(\omega,\theta) d\omega d\theta \tag{5}$$

In the equation above, $H_{\eta x}$ is the transfer function of x and $S_{\eta\eta}$ is the wave spectrum. The latter is calculated distributing the energy of a mono-directional spectrum about the mean wave direction, θ_m, through a spreading function T:

$$T(\theta) = \gamma(s) \cos^{2s}\left[\frac{1}{2}(\theta_m - \theta) \right] \tag{6}$$

where coefficients s and γ depend on the mean wave directional spreading [19]. If the wave elevation is a Gaussian process, so it is the response variable x and the response crest heights, x_c, follow a cumulative Rayleigh distribution F. The distribution of the extreme maximum, F_E, is then calculated as [16], [19]:

$$F_E(x_c) = F(x_c)^N = \left[1 - e^{-(x_c/2\sigma_x)^2} \right]^N \tag{7}$$

where N is the number of response crests, which can be calculated as the ratio between the sea state duration and the response mean zero up-crossing period $T_{x,02}$. From a practical point of view, $F_E(x_c)$ represents the probability that all response crests are below a certain value x_c. Inverting the formula above gives:

$$x_c = \sqrt{2\sigma_x^2} \left[-\ln\left(1 - F_E^{1/N}\right) \right]^{1/2} \tag{8}$$

For a certain value of F_E, which will be called *confidence factor* in the paper, the extreme crest height x_c can thus be calculated and compared to some threshold, to determine whether access is possible or not.

2.3. Evaluation of accessibility

Access with catamaran is possible when the fender does not slip against the boat landing platform mounted on the floating platform. In time domain, the condition of no-slip is written as:

$$\left|\lambda_3(t)\right| \le \mu_s\left[F_b + \lambda_1(t)\right] \tag{9}$$

where λ_1 and λ_3 are, respectively, the horizontal (along x^v-axis) and vertical (along z^v-axis) reaction forces, F_b is the catamaran bollard push force and μ_s is the static friction coefficient at the fender-platform contact surface. This equation can be rewritten as:

$$\alpha(t) = +\lambda_3(t) - \mu_s\lambda_1(t) \le \mu_s F_b \tag{10}$$

$$\beta(t) = -\lambda_3(t) - \mu_s\lambda_1(t) \le \mu_s F_b \tag{11}$$

In addition, it is supposed that personnel transfer cannot be performed when the relative roll ($\Delta\rho$) and yaw ($\Delta\psi$) motions between the two bodies, as seen from the vessel, exceed specific limits. This is written as:

$$\left|\Delta\rho(t)\right| \le \Delta\rho_{\text{lim}} \tag{12}$$

$$\left|\Delta\psi(t)\right| \le \Delta\psi_{\text{lim}} \tag{13}$$

The transfer functions for α, β, $\Delta\rho$ and $\Delta\psi$ are calculated as:

$$\alpha(j\omega) = +\lambda_3(j\omega) - \mu_s\lambda_1(j\omega) \tag{14}$$

$$\beta(j\omega) = -\lambda_3(j\omega) - \mu_s\lambda_1(j\omega) \tag{15}$$

$$\Delta\rho(j\omega) = \zeta_4(j\omega) + \zeta_{10}(j\omega) \tag{16}$$

$$\Delta\psi(j\omega) = \zeta_6(j\omega) - \zeta_{12}(j\omega) \tag{17}$$

For each of these variables the extreme maximum response is calculated, assuming a certain confidence factor, using Equations (5)-(8). The extreme responses are then compared to the respective thresholds, using Equations (10)-(13), to determine whether the platform is accessible or not.

3. Case study: access of a semi-submersible floating platform

3.1. Offshore location and climate

This study considers a site located approximately 15 kilometers off the coast of Aberdeen, Scotland (57.000º N, 1.875º W), where the water depth is 90 m. Wave data is provided by the reanalysis databases of IH Cantabria: this institution has generated a reliable dataset (GOW, Global Ocean Waves [20]) calibrated with satellite information and validated against field data. Data is extracted with hourly resolution for the period from 1980 to 2013. Wave parameters include significant height (H_s), peak period (T_p), mean direction (θ_m) and mean directional spreading (σ_θ). Table 1 and Table 2 show combined Probability Density Functions (PDFs) of wave parameters at the chosen location. In each table, headings represent the value of the bins centers used for the calculation. More than 85% of the time H_s has been lower than 2 m, while two main wave directions are identified: NNE and SE.

Table 1: Scatter diagram for H_s and T_p at Aberdeen, 1980-2013.

		Wave significant height [m]							
		0.5	**1.5**	**2.5**	**3.5**	**4.5**	**5.5**	**6.5**	
Wave peak period [s]	**2**	0.1%	0.0%	0.0%	0.0%	0.0%	0.0%	0.0%	0.1%
	3	1.6%	0.0%	0.0%	0.0%	0.0%	0.0%	0.0%	1.6%
	4	6.9%	0.4%	0.0%	0.0%	0.0%	0.0%	0.0%	7.3%
	5	9.1%	4.5%	0.0%	0.0%	0.0%	0.0%	0.0%	13.6%
	6	7.5%	9.1%	0.6%	0.0%	0.0%	0.0%	0.0%	17.1%
	7	5.5%	7.8%	2.0%	0.0%	0.0%	0.0%	0.0%	15.4%
	8	4.9%	7.3%	3.0%	0.5%	0.0%	0.0%	0.0%	15.7%
	9	3.5%	4.4%	2.3%	1.0%	0.1%	0.0%	0.0%	11.4%
	10	2.2%	2.9%	1.2%	0.6%	0.3%	0.1%	0.0%	7.3%
	11	1.5%	2.1%	0.6%	0.3%	0.1%	0.1%	0.0%	4.6%
	12	0.9%	1.3%	0.4%	0.2%	0.0%	0.0%	0.0%	2.7%
	13	0.5%	0.6%	0.2%	0.1%	0.0%	0.0%	0.0%	1.3%
	14	0.4%	0.3%	0.1%	0.0%	0.0%	0.0%	0.0%	0.9%
	15	0.4%	0.2%	0.0%	0.0%	0.0%	0.0%	0.0%	0.6%
	16	0.2%	0.0%	0.0%	0.0%	0.0%	0.0%	0.0%	0.3%
	17	0.1%	0.0%	0.0%	0.0%	0.0%	0.0%	0.0%	0.1%
		45.3%	40.8%	10.2%	2.7%	0.6%	0.1%	0.0%	100.0%

Table 2: Scatter diagram for H_s and θ_m at Aberdeen, 1980-2013.

			Wave significant height [m]							
			0.5	**1.5**	**2.5**	**3.5**	**4.5**	**5.5**	**6.5**	
Wave mean direction [deg]	**0**	**E**	1.5%	1.5%	0.6%	0.3%	0.1%	0.0%	0.0%	3.9%
	22.5	**ESE**	3.8%	3.2%	1.1%	0.4%	0.2%	0.1%	0.0%	8.8%
	45	**SE**	5.1%	4.5%	1.3%	0.4%	0.1%	0.0%	0.0%	11.3%
	67.5	**SSE**	3.7%	4.3%	1.5%	0.4%	0.1%	0.0%	0.0%	10.0%
	90	**S**	3.0%	3.1%	0.8%	0.1%	0.0%	0.0%	0.0%	7.0%
	112.5	**SSW**	3.9%	3.5%	0.5%	0.1%	0.0%	0.0%	0.0%	7.9%
	135	**SW**	1.3%	1.1%	0.1%	0.0%	0.0%	0.0%	0.0%	2.5%
	157.5	**WSW**	0.4%	0.3%	0.0%	0.0%	0.0%	0.0%	0.0%	0.8%
	180	**W**	0.3%	0.2%	0.0%	0.0%	0.0%	0.0%	0.0%	0.5%
	202.5	**WNW**	0.3%	0.1%	0.0%	0.0%	0.0%	0.0%	0.0%	0.4%
	225	**NW**	0.3%	0.2%	0.0%	0.0%	0.0%	0.0%	0.0%	0.5%
	247.5	**NNW**	0.6%	0.4%	0.0%	0.0%	0.0%	0.0%	0.0%	1.0%
	270	**N**	1.9%	1.5%	0.2%	0.0%	0.0%	0.0%	0.0%	3.6%
	292.5	**NNE**	9.9%	9.9%	2.4%	0.6%	0.1%	0.0%	0.0%	22.9%
	315	**NE**	5.0%	3.2%	0.5%	0.1%	0.0%	0.0%	0.0%	8.9%
	337.5	**ENE**	3.0%	2.3%	0.5%	0.2%	0.0%	0.0%	0.0%	6.0%
			45.4%	40.9%	10.2%	2.7%	0.6%	0.1%	0.0%	100.0%

Finally, Figure 2 illustrates the variation of the mean significant wave height across the months of the year. The continuous line represents the monthly mean H_s (μ) averaged over the years, while the dotted lines the monthly mean H_s plus or minus its standard deviation (μ+σ, μ-σ), averaged over the years. A strong seasonality is ascertained, together with a marked variability during the winter months. July is the month where the wave height tends to be smaller and less variable. As opposite, January is the month where wave height is larger, and more variable.

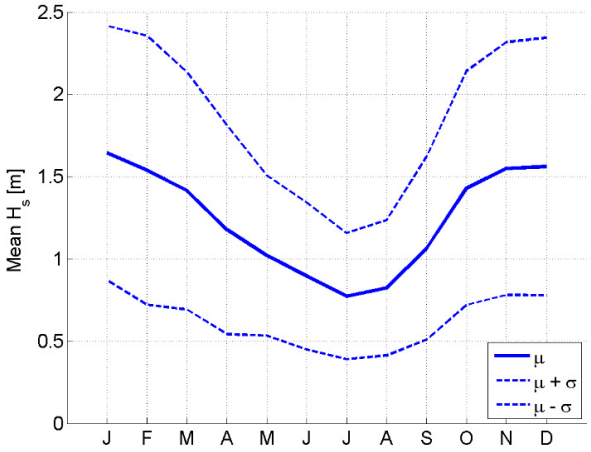

Figure 2: Monthly variation of mean Hs at Aberdeen, 1980-2013.

3.2. Wind turbine and access vessel

The floating platform used in this work is the OC4 semi-submersible, designed by the National Renewable Energy Laboratory [21]. The system is composed by three columns, placed at the vertices of an equilateral triangle and equipped with heave plates. A central column supports the wind turbine tower; columns are connected by pontoons and cross braces. The floating platform is supposed to be accessed by means of a catamaran Crew Transfer Vessel (CTV), which properties are presented. The main properties of the OC4 and the CTV are summarized in Table 3.

Table 3: Main properties of the OC4 and the CTV.

OC4			**CTV**		
Displacement	13473	t	Displacement	102	t
Total draft	20	m	Length/Beam/Draft	24/10/1.37	m
Diameter of central/offset column	6.5/12.0	m	Water plane area	94.45	m^2
Diameter of heave plates	24	m	Vertical centre of gravity	2.95	m
Spacing between offset columns	50	m	Heave/roll/pitch natural periods	3.0/3.5/4.5	s
Heave natural period	18	s	Bollard push force	135	kN
Roll/pitch natural period	27.5	s	Fender friction coefficient	1.2	-

3.3. Multi-body system Response Amplitude Operators (RAOs)

The solution of Equation (3) allows to find the transfer functions of the system. Figure 3 and Figure 4 show the displacements of the CTV and the OC4 respectively, for different wave headings referred to the vessel ("HS" = "Head Sea", "HQS" = "Head Quartering Sea", "BS" = "Beam sea"). Given the large inertia and submerged volume difference, the two bodies would respond differently to different excitation frequencies, if free to move: the CTV is more sensitive to short waves, while the OC4 to longer ones. However, the forces exchanged at the joint affect the combined response of the two bodies. Evidently, it is the OC4 that influences more the response of the CTV, and not vice versa.

Figure 5 shows reaction forces at the joint, and the variables α and β, see Equations (14)-(15). Vertical reaction forces are usually larger than horizontal forces, especially for large wave periods. It is worth noticing that, for small

wave periods, the response of α is larger than that of β which means that, in this region, upward slip is more probable than downward slip. Finally, it is important to observe that largest motions and reaction forces occur at wave periods (16.5 s and 24.0 s) which do not match exactly the OC4 natural periods (18.0 s and 27.5 s, see Table 3): this is because it is the relative motion between the two bodies, and not the absolute one, that drives contact forces and thus the response of the system.

Finally, Figure 6 presents the maximum wave height for which access is possible, under the hypothesis of regular waves, in a polar diagram. The radial coordinate represents the wave period, while the angular coordinate the wave heading with respect to the CTV. For short wave periods, the best performance is obtained for beam seas, which correspond to low reaction forces. It would be interesting to repeat the calculations including second order wave forces and considering large displacements, in order to evaluate the validity of results without the limitations of frequency domain modelling. Nevertheless, these findings are in line with others in literature, which refer to fixed wind turbines [11]. For longer waves, head seas are preferable to beam seas. It can be noticed that, in general, head seas facilitate accessibility more than following seas, due to the presence of the floating platform which absorbs or reflects part of the incoming waves. The poor accessibility for wave periods which correspond to the highest OC4 heave response is evident, regardless of the wave heading.

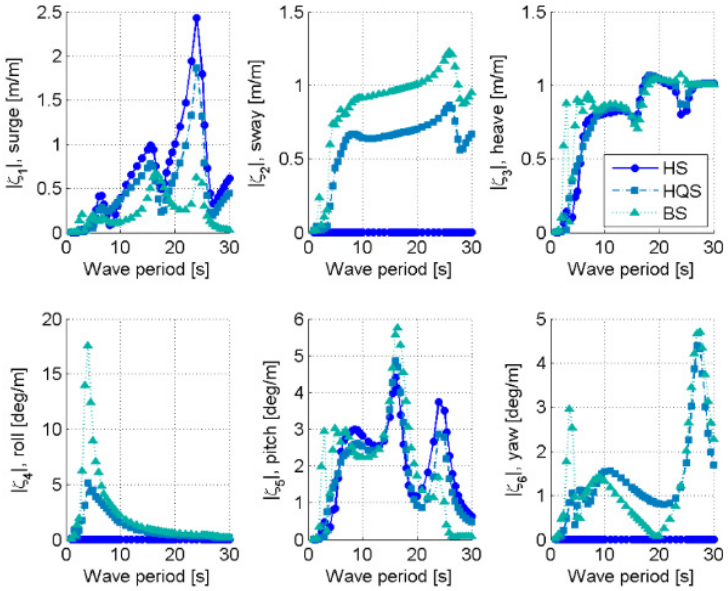

Figure 3: RAOs for CTV displacement, CTV-OC4 walk-to-work configuration

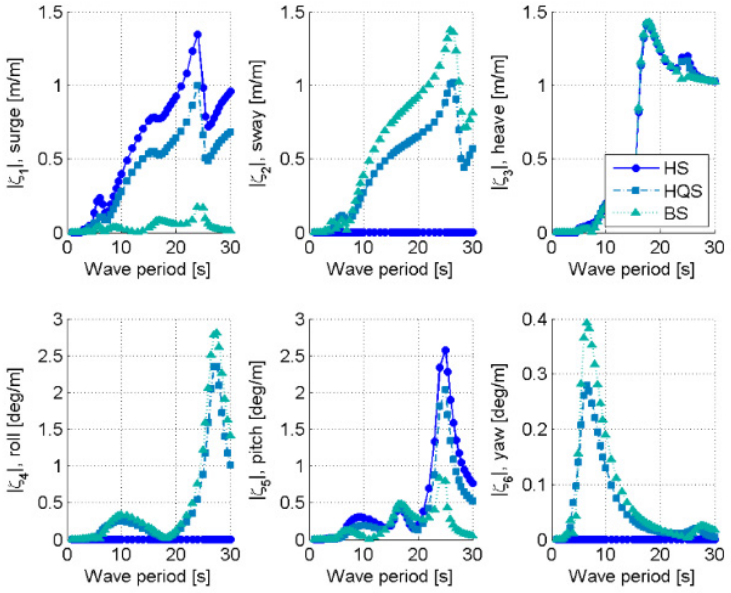

Figure 4: RAOs for OC4 displacement, CTV-OC4 walk-to-work configuration

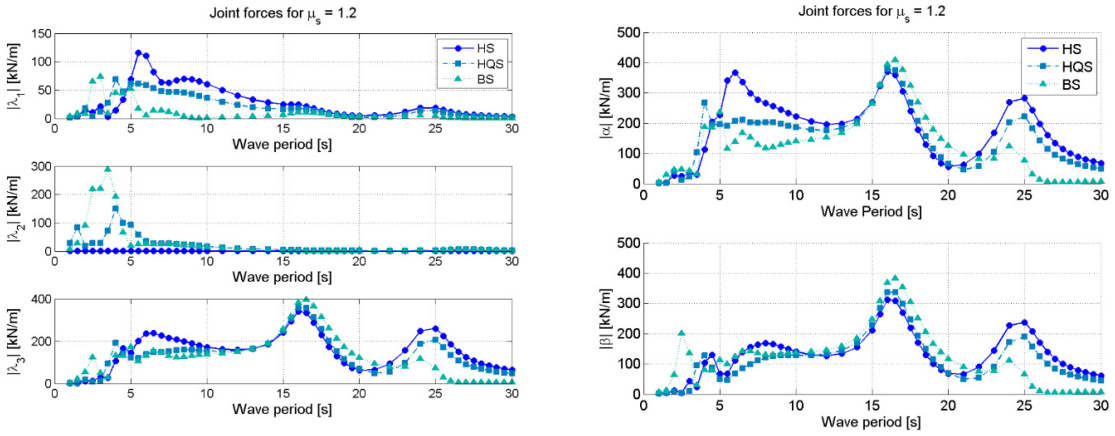

Figure 5: RAOs for contact forces at fender (left) and α and β (right), CTV-OC4 walk-to-work configuration

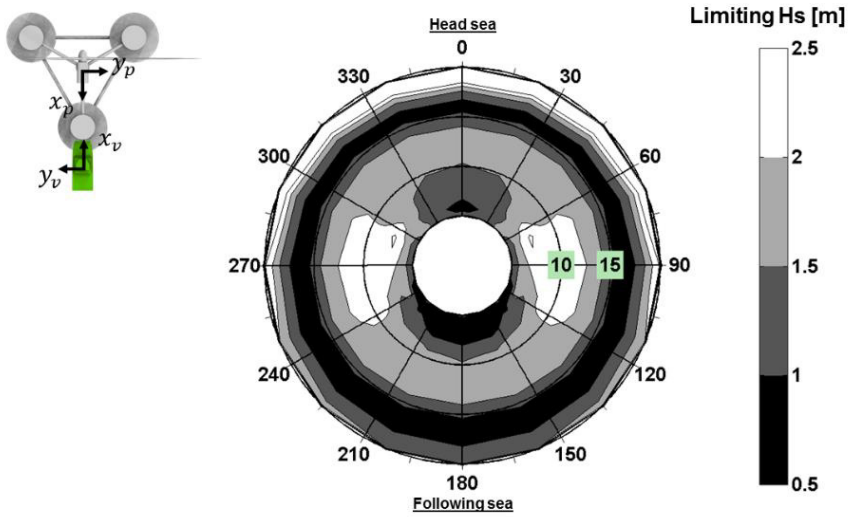

Figure 6: Limiting wave height for regular waves, CTV-OC4 walk-to-work configuration. Radial coordinate is wave peak period, angular coordinate is wave heading with respect to the vessel.

3.4. Long-term accessibility

The available hindcast data has been used to calculate accessibility in the period 1980-2013, applying Equations (5)-(8) for each hourly sea state assuming JONSWAP spectra with shape factor equal to 3.3. The maximum allowable relative roll/yaw rotation has been set to 5 degrees, see Equations (12)-(13), while the confidence factor F_E is 0.95.

The mean accessibility for the studied 34 years period resulted to be 23.7%. Figure 7 (left) illustrates results for the monthly accessibility, including mean values (μ), mean plus or minus standard deviation (μ+σ, μ-σ), minimum (min) and maximum (max) values registered over the considered period. Consistently with the wave height regime (see Figure 2), accessibility is higher during summer (being July the month with highest accessibility), and much lower during winter (being January the month with the lowest accessibility). A very strong variability is observed, which depends on the variability of wave climate at Kincardine: this emphasizes the need for long-term, reliable data in order to reduce uncertainty when designing operation and maintenance strategies for offshore wind farms. It is important to notice that variability is marked during summer months, more than during winter months (differently from what happens for the wave height regime). This is because mean wave height during winter is far above the limits that the CTV can stand, and a variation about this value does not change significantly the probability of access. As opposite, during summer months, the mean wave height is in an admissible range for the CTV, and a variation about this value can dramatically change accessibility.

Figure 7 (right) depicts the seasonal variation of accessibility with wave height. As expected, accessibility shows a decreasing trend, when the mean wave height increases. Results are more dispersed when H_s is around 1.5 m, when also other parameters such as wave direction, spreading and peak period play a relevant role in the response of the vessel. For wave heights much smaller/higher, access is always/never possible and wave direction and peak period do poorly influence results.

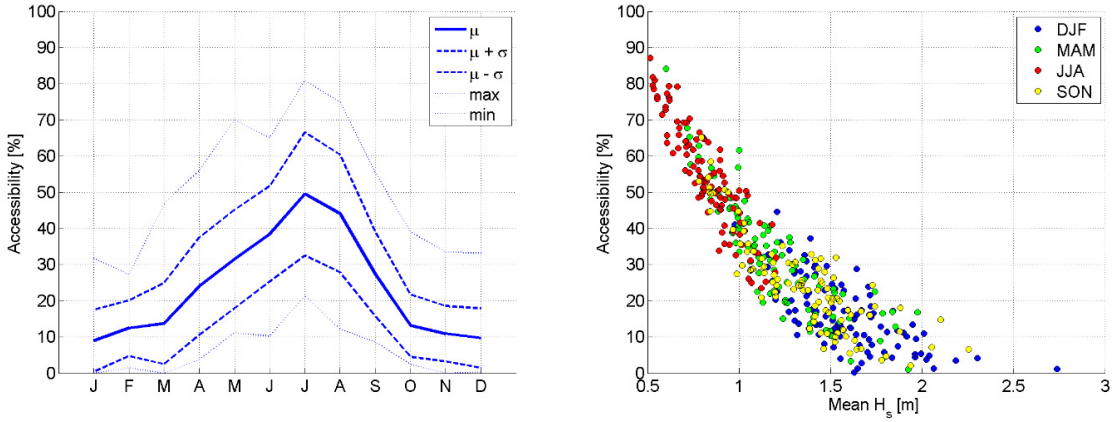

Figure 7: Monthly accessibility distribution (left) and variation with H_s (right) at Kincardine, CTV-OC4 configuration; 1980-2013.

4. Conclusions

In this work, we presented a methodology for estimating the walk-to-work accessibility of a semi-submersible floating wind turbine by means of a catamaran vessel. Using a frequency domain approach, it has been possible to calculate the transfer functions for the combined response of the two bodies, and the forces exchanged at the fender. Findings indicate that the response of the vessel is importantly affected by the motions of the platform, especially when the motions of the latter is expected to be large. Contact forces are larger when the relative motion of the two bodies would be larger, if they were free to move. Access is considered possible when no-slip conditions occur at the fender, and when the relative rotations of the two bodies are within a certain tolerance. For short, regular waves beam seas provide the best configuration for access. For longer waves, head seas are preferable, also taking advantage of the platform shielding effect. Accessibility has been calculated for an offshore location in Scotland, using 34 years of hindcast data with hourly resolution. On average, the chosen site resulted to be accessible for 23.7% of the time. July is the month in which access is more probable (50% of the time, on average), while January the month in which access is less probable (9% of the time). A very large uncertainty associated with those values has been calculated, which highlights the importance of long-term reliable data to correctly design offshore maintenance strategies.

Acknowledgments

The authors would like to acknowledge the projects “OceaNET”, which received funding from the European Union’s Seventh Framework Programme for research, technological development and demonstration under grant agreement no 607656, and “Plataformas multiuso para aplicaciones offshore” of the University of Cantabria (code: 56.JS05.64061).

References

[1] European Wind Energy Association, “The European offshore wind industry – key trends and statistics 1st half 2015,” 2015.
[2] European Wind Energy Association, “Deep water - The next step for offshore wind energy,” 2013.
[3] Statoil, “Hywind Scotland Pilot Park,” 2015. [Online]. Available: http://www.statoil.com/en/TechnologyInnovation/NewEnergy/RenewablePowerProduction/Offshore/HywindScotland. [Accessed: 08-Oct-2015].
[4] Principle Power, “WindFloat Pacific,” 2015. [Online]. Available: http://windfloatpacific.com/. [Accessed:

08-Oct-2015].
[5] Mitsubishy Heavy Industries, “Fukushima experimental offshore floating wind farm project second phase update,” 2015. [Online]. Available: http://www.mhi-global.com/news/story/150622en.html. [Accessed: 19-Oct-2015].
[6] GL Garrad Hassan, “Offshore Wind - Operations and maintenance opportunities in Scotland - An insight into opportunities for Scottish ports and the O&M supply chain,” 2013.
[7] S. Butterfield, W. Musial, J. Jonkman, and P. Sclavounos, “Engineering challenges for floating offshore wind turbines,” National Renewable Energy Laboratory. NREL/CP-500-38776. Golden, CO, USA, 2007.
[8] G9 Offshore Wind Health and Safety, “Good practice guideline working at height in the offshore wind inustry,” 2014.
[9] International Marine Contractors Association, “Transfer of personnel to and from offshore vessels,” 2010.
[10] Sgurr Energy Ltd., “Offshore wind and marine energy health and safety guidelines,” 2014.
[11] M. Wu, “Numerical analysis of docking operation between service vessels and offshore wind turbines,” *Ocean Eng.*, vol. 91, pp. 379–388, 2014.
[12] D. González, M. Lemmerhirt, M. Abdel-Maksoud, M. Konig, and A. Duster, “Numerical and experimental investigation regarding the landing of a catamaran vessel at an offshore wind turbine in waves,” in *ASME 34th International Conference on Ocean, Offshore, and Arctic Engineering*, 2015.
[13] W. E. Cummins, “The impulse response function and ship motions,” in *Symposium on Ship Theory*, 1962.
[14] T. Ogilvie, “Recent progress towards the understanding and prediction of ship motions,” in *5th Symposium on Naval Hydrodynamics*, 1964.
[15] T. I. Fossen, *Handbook of Marine Craft Hydrodynamics and Motion Control*. Trondheim, Norway: John Wiley & Sons, 2011.
[16] Det Norske Veritas, “Environmental Conditions and Environmental Loads,” DNV-RP-C205, 2010.
[17] M. Masciola, “Instructional and theory guide to the Mooring Analysis Program,” Boulder, CO, 2013.
[18] L. Sun, R. Eatock Taylor, and Y. S. Choo, “Response of interconnected floating bodies,” *IES J. Part A Civ. Struct. Eng.*, vol. 4, no. 3, pp. 143–156, 2011.
[19] L. H. Holthuijsen, *Waves in Oceanic and Coastal Waters*. New York: Cambridge University Press, 2007.
[20] B. G. Reguero, M. Menéndez, F. J. Méndez, R. Mínguez, and I. J. Losada, “A Global Ocean Wave (GOW) calibrated reanalysis from 1948 onwards,” *Coast. Eng.*, vol. 65, pp. 38–55, 2012.
[21] A. Robertson, J. Jonkman, M. Masciola, H. Song, A. Goupee, A. Coulling, and C. Luan, “Definition of the semisubmersible floating system for phase II of OC4,” National Renewable Energy Laboratory. NREL/TP-5000-60601. Golden, CO, USA, 2014.